JOURNAL OF APPLIED PHYSICS **116**, 034504 (2014)

Importance of growth direction in mid-infrared quantum cascade lasers

Pierre M. Bouzi,[1,a)] YenTing Chiu,[1,b)] Christoph Deutsch,[1,c)] Yamac Dikmelik,[2] Yu Song,[1] Vadim Tokranov,[3] Serge Oktyabrsky,[3] and Claire Gmachl[1]

[1]*Department of Electrical Engineering, Princeton University, Princeton, New Jersey 08544, USA*
[2]*Department of Electrical and Computer Engineering, Johns Hopkins University, Baltimore, MD 21218, USA*
[3]*College of Nanoscale Science and Engineering, University at Albany-SUNY, Albany, New York 12222, USA*

(Received 7 May 2014; accepted 3 July 2014; published online 16 July 2014)

We report on the effect of growth direction on the performance of mid-infrared Quantum Cascade lasers. The design used has a symmetric active core, capable of operating under both negative and positive polarities, which allows to test for residual growth asymmetries such as interface roughness and dopant migration. Calculations of scattering lifetimes from interface roughness and ionized impurities suggest a dominant contribution from the former, with devices biased positively averaging ~15% larger broadening and ~50% shorter upper state lifetime than negatively biased devices. Experimental results for positively biased devices show at least 30% larger broadening and 35% lower electroluminescence peak intensity than those biased negatively, in good agreement with the modeling results. © *2014 AIP Publishing LLC*. [http://dx.doi.org/10.1063/1.4890311]

I. INTRODUCTION

Quantum Cascade (QC) lasers are unipolar semiconductor devices for the entire mid-infrared (mid-IR) portion of the electromagnetic spectrum. They are traditionally grown via molecular beam epitaxy (MBE)[1,2] or metal organic chemical vapor deposition (MOCVD)[3,4] and operate conventionally under negative bias, with electrons moving against the growth direction. Bi-directional mid-IR QC devices, capable of operating under both negative and positive bias, have been reported.[5] Despite various efforts to eliminate any possible asymmetry in design and fabrication, there remain some inherent asymmetries from QC structure growth, arising from interface roughness between wells and barriers, and asymmetric doping profile from dopant migration.[6] Such growth-induced asymmetries have been investigated in III-V semiconductor heterostructures and extensively studied in the InAs/GaSb material system.[7] Recently, the effect of asymmetric interfaces[8] and dopant migration[9] has also been studied in terahertz (THz) QC lasers with InGaAs/GaAsSb lattice-matched to InP and GaAs/AlGaAs grown on GaAs substrate, respectively. In both cases, symmetric active regions were employed and a large disparity in performance was reported for devices under different polarities.

Small interface roughness asymmetries have been reported between AlGaAs and GaAs in MBE grown two-dimensional systems.[10] And, adopting a similar argument as discussed in Ref. 10, one can conclude that the InGaAs-on-InAlAs interface is rougher on the atomic level when compared to the AlInAs-on-InGaAs interface. Due to their lower atomic mobility compared to Ga atoms, Al atoms localize during the growth of InAlAs and induce roughness that accumulates up to the InGaAs-on-InAlAs interface. The roughness is then smoothed out in the presence of the very mobile Ga atoms during the growth of InGaAs. Recently, Lopez *et al*. reported on the direct measurement of interface roughness in InGaAs/InAlAs QC lasers grown by MOCVD and found that InGaAs-on-InAlAs heterojunctions are rougher and more strongly correlated than InAlAs-on-InGaAs ones.[11]

II. SYMMETRIC ACTIVE REGIONS

Here, we investigate the impact of growth direction on the performance of mid-IR QC devices by using a symmetric active region and injector structure that can be biased in both polarities. This is a very simple and effective approach to testing the residual structure asymmetry in growth, as only one structure needs to be grown, thereby eliminating possible variations that may occur during multiple growth runs. Figure 1 shows the symmetric QC structure grown by MBE using lattice-matched $In_{0.53}Ga_{0.47}As/In_{0.52}Al_{0.48}As$ on InP substrate. It is a two-well active region and short-injector design, with the optical transition between states 3 and 2 indicated by the wavy arrow. The same structure is shown under negative and positive bias, with a design wavelength of 7.2 μm. The strict symmetry constraint results in a short period design (36 nm) and diagonal transition with a long longitudinal optical (LO) phonon scattering lifetime (~80 ps) for the upper state. The dashed lines represent the nominal doping profile, and the shaded region indicates dopant migration, which has been reported to occur along the growth direction with a characteristic migration length that depends on growth temperature.[12] The rough lines along the interfaces between the quantum wells and barriers illustrate an inherent interface roughness (IFR) asymmetry when InGaAs is grown on InAlAs. Under applied bias, the nominally symmetric band structure becomes asymmetric as the upper state wave functions overlap more with the migrating dopants depending on the bias polarity and differently doped regions. In addition, as the wavefunctions shift in different

[a)]Email: pbouzi@princeton.edu.
[b)]Current address: Intel Oregon, Portland Technology Development, Hillsboro, OR 97124, USA.
[c)]Permanent address: Photonics Institute, Vienna University of Technology, Gusshausstrasse 27-29/387, A-1040 Vienna, Austria.

 © 2014 AIP Publishing LLC

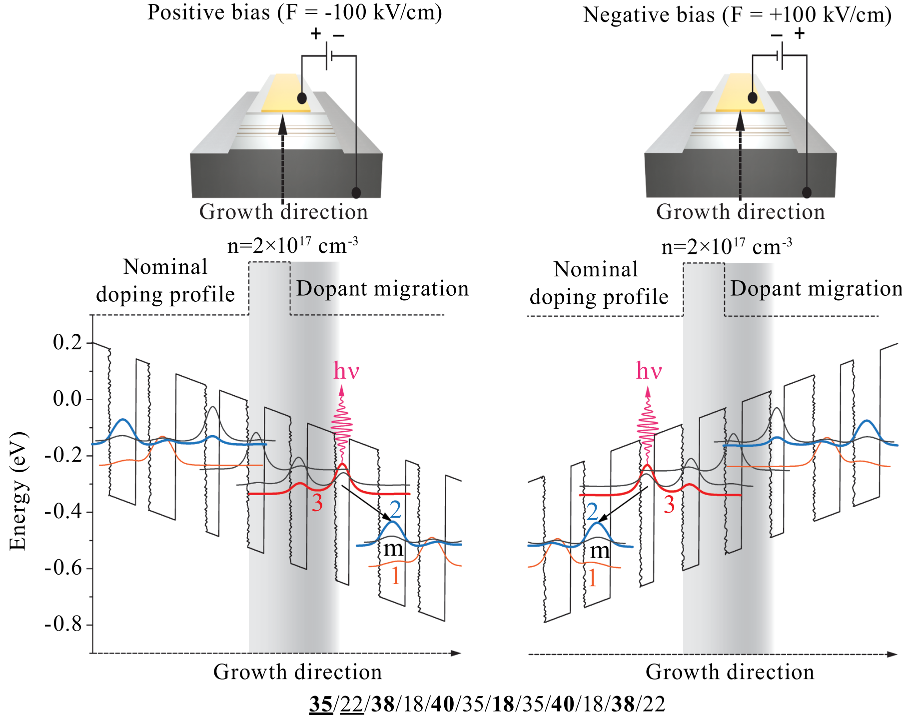

FIG. 1. Band structure diagrams of a symmetric QC device at 100 kV/cm. The optical transition, indicated by the wavy arrow, is designed at 7.2 μm and occurs between states 3 and 2 highlighted in red and blue, respectively. Subband state 1 is the depopulation state and state *m* is localized in the injector region. The same design is shown for both polarities, with the shaded region highlighting the dopant migration profile. The rough lines between each well and barrier indicates the greater roughness which occurs when InGaAs is grown on AlInAs. The nominal layer thicknesses are shown at the bottom, with the doped (2×10^{17} cm^{-3}) layers underlined. The diagrams on top of the band structures indicate the bias polarity, along with the corresponding field.

directions under different polarities, they overlap more with either the rough or the smooth interfaces, resulting in an additional asymmetry.

III. SIMULATION RESULTS

Interface roughness scattering in QC lasers has been shown to affect intersubband absorption,[13] intersubband broadening,[14] and transport mechanism via resonant tunneling.[15] Here, to estimate the effect of inter- and intra-subband scattering induced by asymmetric interfaces on our device performance under different polarities, we follow Ref. 14:

$$\Gamma^{IFR}_{intra}(E) = \frac{\pi m^*}{\hbar^2}\delta U^2\left\{\Delta_1^2\Lambda_1^2\sum_{i,1}[\varphi_m(z_{i,1})^2 - \varphi_n(z_{i,1})^2]^2 + \Delta_2^2\Lambda_2^2\sum_{i,2}[\varphi_m(z_{i,2})^2 - \varphi_n(z_{i,2})^2]^2\right\}, \tag{1.1}$$

$$\Gamma^{IFR}_{inter}(E) = \frac{\pi m^*}{\hbar^2}\delta U^2\left\{\Delta_1^2\Lambda_1^2\sum_{i,1}[\varphi_m(z_{i,1})\varphi_n(z_{i,1})]^2 e^{\frac{-\Lambda_1^2 q_{mn}^2}{4}} + \Delta_2^2\Lambda_2^2\sum_{i,2}[\varphi_m(z_{i,2})\varphi_n(z_{i,2})]^2 e^{\frac{-\Lambda_2^2 q_{mn}^2}{4}}\right\}. \tag{1.2}$$

Here, m* is the effective mass and δU the conduction band offset. Δ_1, Λ_1, $z_{i,1}$ and Δ_2, Λ_2, $z_{i,2}$ are the roughness heights, correlation lengths and locations for InGaAs-on-AlInAs and AlInAs-on-InGaAs interfaces, respectively. φ_m and φ_n are the upper and lower state wavefunction amplitudes at the interfaces, respectively, and q_{mn} is absolute value of the 2D scattering vector in this process.[14]

We calculate the scattering time then as:

$$\tau^{IFR}_{intra/inter} = \frac{\hbar}{\Gamma^{IFR}_{intra/inter}(E)}, \tag{1.3}$$

where τ is the scattering time, $\hbar$ the reduced Planck constant and Γ^{IFR}_{intra} and Γ^{IFR}_{inter} the broadenings of intra- and inter-subband transitions, respectively.

Ionized impurity scattering (IMP) is also considered. While mid-IR QC structures are usually doped in the injector region, a migration of dopant atoms in the direction of crystal growth may occur depending on the growth conditions, especially the growth temperature.[12] The origin of such a migration is either attributed to surface electric field-enhanced diffusion during growth[16] or surface segregation as discussed in Ref. 10. As a result, the dopant distribution may reach part of the active region and affect the optical transition. As can be seen in Fig. 1, when the device is biased positively, the upper state overlaps more with the dopants, with an expected lifetime reduction of the upper level[17] and broadening.[18] In order to investigate and quantify this scattering process, we assume that the impurity density is low enough so that each individual impurity can be treated separately from the others, and the screening effect is ignored. The intra- and inter-subband scattering lifetime induced by ionized impurity scattering can then be calculated as:

$$\tau^{IMP}_{intra/inter} = \frac{\hbar}{\Gamma^{IMP}_{intra/inter}(E)}, \tag{2.1}$$

where Γ^{IMP}_{intra} and Γ^{IFR}_{inter} are broadenings given by:[14]

$$\Gamma^{IMP}_{intra}(E) = \frac{m^* e^4}{4\epsilon_0^2 \epsilon_r^2 \hbar^2} \int dZ_{imp} N(Z_{imp}) \times \left\{ \frac{1}{\tilde{q}} \int dz [\varphi_m(z)^2 - \varphi_n(z)^2] e^{-\tilde{q}|z - Z_{imp}|} \right\}^2, \quad (2.2)$$

$$\Gamma^{IMP}_{inter}(E) = \frac{m^* e^4}{4\epsilon_0^2 \epsilon_r^2 \hbar^2} \int dZ_{imp} N(Z_{imp}) \times \left\{ \frac{1}{q} \int dz [\varphi_m(z) \varphi_n(z)] e^{-q|z - Z_{imp}|} \right\}^2, \quad (2.3)$$

where e is the electronic charge, ϵ_0 the permittivity of free space and ϵ_r the relative permittivity of the material system. $N(Z_{imp})$ is the 3D impurity concentration at position Z_{imp} and q and $\tilde{q}$ are the absolute values of the 2D intra- and inter-subband scattering vectors.[14,19]

Figure 2 shows the calculation results versus electric field for intersubband scattering lifetime induced by IMP and IFR under both polarities. For IMP, we performed the calculations for a wide range of migration lengths (1–15 nm). However, here we only show the result for a migration length of 4 nm, where the overlap of the upper state wavefunction with migrating dopants is becoming pronounced under positive bias, as shown in Fig. 1. Due to more interaction with migrating dopants, the IMP scattering lifetime of positively biased devices is much shorter than that of negatively biased ones. However, in both cases, the lifetime remains much longer than the longitudinal optical (LO) phonon scattering lifetime, which is why IMP scattering is usually ignored in mid-IR QC devices.[16]

For IFR, we assume a value of 6 nm for the correlation length and roughness heights of 0.2 nm and 0.1 nm for rough and smooth interfaces, respectively. Similar values have been used recently and resulted in good agreement with experimental data.[20] The IFR scattering lifetime for devices under positive bias is about half that of negatively biased devices, and they both fall below the LO phonon scattering lifetime. As such, IFR scattering under both polarities is expected to have a significant contribution to the total scattering process.

Fig. 3(a) shows the electric field-dependent intra-subband broadening induced by IMP and IFR under both polarities, with the same parameters as those used in Fig. 2. While the magnitude of IMP intra-subband broadening is relatively small, devices biased positively result in a broadening about 50% greater that calculated under negative bias. For IFR, the calculated intra-subband broadening is dominant, with 15% greater values for positively biased devices compared to those under negative polarity. The combined broadening from IMP and IFR is shown in Fig. 3(b), with a ~20% difference between devices biased positively and negatively, as shown on the right axis. The small peak that occurs around 105 kV/cm is attributed to states 2 and m being in resonance, resulting in a larger transition broadening from delocalization across more interfaces.

While these results are specific to the design structure considered here, we expect a similar effect of asymmetry on more generic structures, including high performance devices

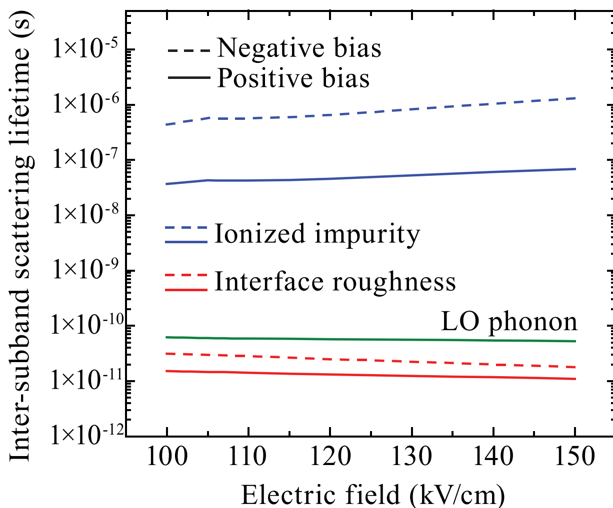

FIG. 2. IFR and IMP effective upper state scattering lifetimes versus electric field, under negative and positive bias. For IMP, we use a migration length of 4 nm and for IFR, a correlation length of 6 nm is chosen along with roughness heights of 0.1 nm and 0.2 nm for the smooth and rough interfaces, respectively. The green line indicates the LO phonon effective upper state scattering lifetime.

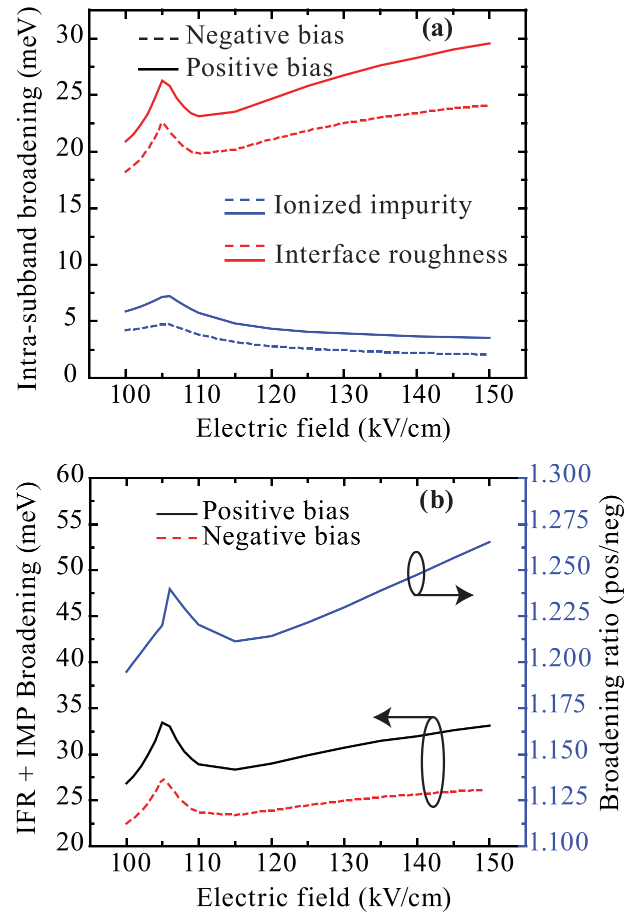

FIG. 3. (a) Broadening induced by IMP and IFR scattering calculated at various electric fields, under negative and positive bias, assuming the same structure asymmetry as in Fig. 2. (b) Total broadening induced by both IFR and IMP, calculated versus electric field, under negative and positive bias. The right axis shows the ratio of positive and negative broadening versus electric field. The peak around 105 kV/cm occurs as a result of states 2 and m coming in resonance, resulting in a larger transition broadening.

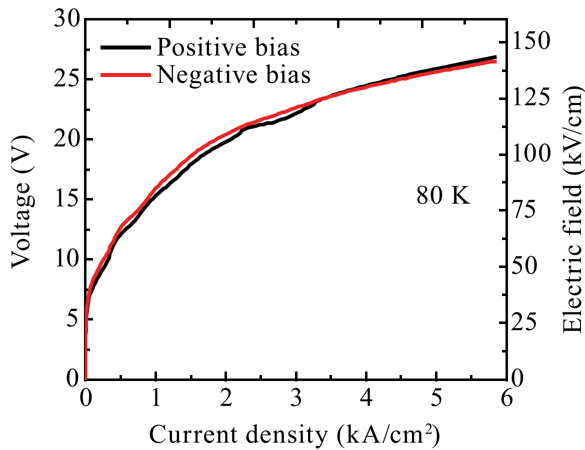

FIG. 4. Voltage-current characteristics of a circular mesa device with 200 μm diameter at 80 K under both polarities. The contacts have been annealed to reduce parasitic voltage drops outside the active core.[21]

which have much shorter phonon-limited lifetimes ($\sim$1 ps). In fact, Ref. 20 presents results on more than 20 of such devices, where interface roughness and phonon scattering lifetimes have similar magnitudes. In addition, asymmetry-induced broadening is expected to affect device performance, irrespective of phonon scattering.

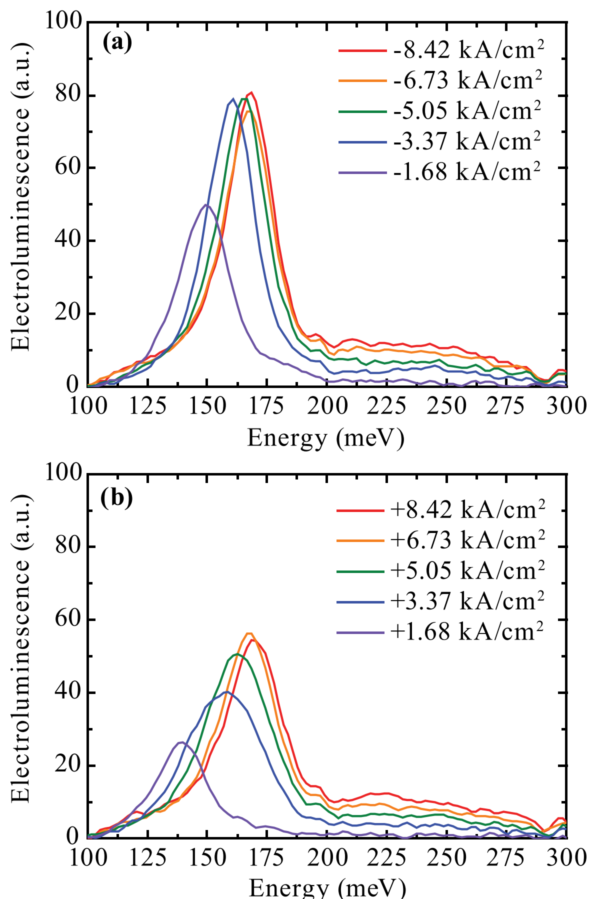

FIG. 5. Electroluminescence spectra of a semi-circular mesa device at various current levels under negative (a) and positive (b) bias, respectively. The measurements were taken at 80 K with a pulsed power supply with 100 ns pulse width and 5 kHz repetition rate. The corresponding electric field range varies from 105 kV/cm to 150 kV/cm.

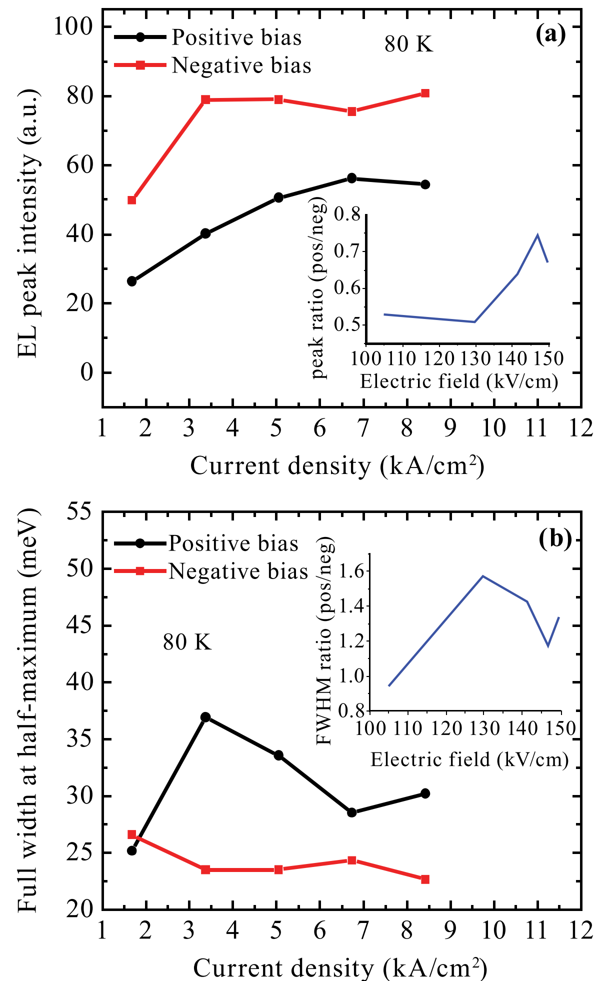

FIG. 6. (a) Peak EL intensity extracted from Fig. 5 under both polarities. The inset shows the ratio of their peak intensity with a maximum 50% difference in favor of negative bias on the devices. (b) Full width at half-maximum of the EL spectra shown in Fig. 5, plotted versus current density under both polarities. The inset shows the ratio of broadening between positive and negative bias.

IV. FABRICATION AND EXPERIMENTAL RESULTS

In order to experimentally quantify growth-related performances, we have processed and characterized the symmetric structure afore mentioned under both polarities. We fabricated several circular mesa devices of $\sim$200 μm diameter, using standard optical lithography and wet-chemical etching (10:1:1 = H_2O: HBr: HNO_3), similar to Ref. 21. This step was then followed by the deposition of thin layers of Ti/Au (200 Å/2000 Å) on degenerately doped ($2 \times 10^{19}\,cm^{-3}$) InGaAs layers, thereby forming an ohmic contact at the metal-semiconductor junction. The bottom contact consists of the low-doped ($1 \times 10^{17}\,cm^{-3}$) InP substrate with a Ge/Au (300 Å/2000 Å) metal contact, forming a Schottky barrier that requires $\sim$1V turn-on voltage. To reduce possible asymmetry introduced by the contacts, we employed rapid thermal annealing (RTA) on our contacts.

Fig. 4 shows the current-voltage (I-V) characteristics of a circular device at 80 K under both polarities, with 0.5 V subtracted to account for parasitic voltage drop outside the active core.[22] The data were obtained with a pulsed power supply with 100 ns pulse width and 5 kHz repetition rate. The

resulting I-V curves do not fall exactly on top of each other, which indicates some asymmetry in electron flow through the device. The small waviness is reproduced across devices.

Figs. 5(a) and 5(b) show the electroluminescence (EL) spectra of a cleaved semi-circular sample with 200 μm diameter at various current densities and under negative and positive polarity. While the emission peaks around the designed wavelength (7.2 μm) in both polarities, the peak intensity under negative bias across a wide field range is at least 35% higher than that for positive bias, as shown in Fig. 6(a) and inset. The full width at half maximum (FWHM) measured in both polarities is shown in Fig. 6(b), with positively biased devices averaging ∼30% larger values than those measured under negative bias across various fields.

The experimental results qualitatively agree with our model in two main aspects. First, the calculated intersubband IFR lifetime is shorter for positively biased devices compared to those biased negatively, which is consistent with the differences in measured peak intensities in both polarities, as the lesser EL peak intensity indicates a shorter lifetime. Second, the calculated field dependent IFR and IMP broadenings in both polarities again qualitatively agree with the FWHM measurements in that the FWHM of the positive polarity sample is greater, with a magnitude (20–30 meV) that generally agrees with the model. In addition, the broadening ratio calculated between positively and negatively biased devices and shown in the inset of Fig. 6(b) has the same order of magnitude as the measured one shown in the inset of Fig. 3(b).

V. CONCLUSION AND OUTLOOK

In summary, we have designed, grown, and characterized symmetric QC devices to investigate the effect of growth direction on the performance of mid-IR QC lasers. Calculations of LO phonon, IMP and IFR inter- and intra-subband scattering lifetimes reveal a dominant IFR contribution to the device transport characteristics and EL in both polarities, with ∼15% larger broadening and ∼50% shorter upper state lifetime for devices under positive polarity compared to those biased negatively. These results are in good agreement with the experimental data, with devices measured under positive bias reaching EL peak intensities at least 35% lower and FWHM at least 15% higher than those measured under negative bias. While the contribution of IMP intra-subband broadening can be minimized via doping setbacks,[8,23] the dominating results calculated for IFR inter- and intra-subband scattering under both polarities reveal its effect on device performance and its dependence on growth direction. As such, given a design structure, IFR scattering calculations should serve as a guide to structure growth direction.

While we present results for EL structures here, the design can be optimized to produce working lasers as well. In fact, lasing has already been demonstrated for a mid-IR symmetric QC structure in Ref. 5. Next, we plan to tailor the interface roughness to further optimize QC laser performance.

ACKNOWLEDGMENTS

The authors would like to acknowledge Igor Trofimov for his assistance with the wafers, Arvind Ravikumar for helpful discussions on the simulation model, and the funding support from MIRTHE (NSF-ERC) and NSF, Contract No. ECCS-1236459.

[1]H. Beere, J. Fowler, J. Alton, E. Linfield, D. Ritchie, R. Kohler, A. Tredicucci, G. Scalari, L. Ajili, J. Faist, and S. Barbieri, J. Cryst. Growth **278**(1–4), 756 (2005).
[2]F. Q. Liu, L. Li, L. J. Wang, J. Q. Liu, W. Zhang, Q. D. Zhang, W. F. Liu, Q. Y. Lu, and Z. G. Wang, Appl. Phys. A **97**, 527 (2009).
[3]Z. Liu, D. Wasserman, S. S. Howard, A. J. Hoffman, C. F. Gmachl, X. Wang, T. Tanbun-Ek, L. Cheng, and F. S. Choa, IEEE Photon. Technol. Lett. **18**(12), 1347–1349 (2006).
[4]J. C. Shin, M. D'Souza, J. Kirch, J. H. Park, L. J. Mawst, and D. Botez, J. Cryst. Growth **312**, 1379–1382 (2010).
[5]C. Gmachl, A. Tredicucci, D. L. Sivco, A. L. Hutchinson, F. Capasso, and A. Y. Cho, Science **286**, 749 (1999).
[6]H. C. Liu, Z. R. Wasilewski, M. Buchanan, and H. Chu, Appl. Phys. Lett. **63**, 761 (1993).
[7]R. M. Feenstra, D. A. Collins, D. Z. Y. Ting, M. W. Wang, and T. C. McGill, Phys. Rev. Lett. **72**, 2749 (1994).
[8]C. Deutsch, H. Detz, T. Zederbauer, A. M. Andrews, P. Klang, T. Kubis, G. Klimeck, M. E. Schuster, W. Schrenk, G. Strasser, and K. Unterrainer, Opt. Express **21**(6), 7209–7215 (2013).
[9]C. Deutsch, H. Detz, M. Krall, M. Branstetter, T. Zederbauer, A. M. Andrews, W. Schrenk, G. Strasser, and K. Unterrainer, Appl. Phys. Lett. **102**, 201102 (2013).
[10]H. Morkoc, T. J. Drummond, and R. Fischer, J. Appl. Phys. **53**, 1030 (1982).
[11]F. Lopez, M. R. Wood, M. Weimer, C. F. Gmachl, and C. G. Caneau, "Direct measurement of interface roughness in QCL materials grown by MOCVD," in *International Conference on Intersubband Transitions in Quantum Wells (ITQW)*, Bolton Landing, NY, September 2013.
[12]M. Santos, T. Sajoto, A. Zrenner, and M. Shayegan, Appl. Phys. Lett. **53**, 2504 (1988).
[13]K. L. Campman, H. Schmidt, A. Imamoglu, and A. C. Gossard, Appl. Phys. Lett. **69**, 2554 (1996).
[14]T. Unuma, T. Takahashi, T. Noda, M. Yoshita, H. Sakaki, M. Baba, and H. Akiyama, Appl. Phys. Lett. **78**, 3448 (2001).
[15]J. B. Khurgin, Y. Dikmelik, P. Q. Liu, A. J. Hoffman, M. D. Escarra, K. J. Franz, and C. F. Gmachl, Appl. Phys. Lett. **94**, 091101 (2009).
[16]E. F. Schubert, J. M. Kuo, R. F. Kopf, A. S. Jordan, H. S. Luftman, and L. C. Hopkins, Phys. Rev. B **42**, 1364 (1990).
[17]R. Ferreira and G. Bastard, Phys. Rev. B **40**, 1074 (1989).
[18]J. Faist, F. Capasso, C. Sirtori, D. L. Sivco, A. L. Hutchinson, S. N. G. Chu, and A. Y. Cho, Appl. Phys. Lett. **65**, 94 (1994).
[19]T. Ando, J. Phys. Soc. Jpn. **54**, 2671 (1985).
[20]Y. Chiu, Y. Dikmelik, P. Q. Liu, N. L. Aung, J. B. Khurgin, and C. Gmachl, Appl. Phys. Lett. **101**, 171117 (2012).
[21]M. D. Escarra, A. Benz, A. M. Bhatt, A. J. Hoffman, X. Wang, J. Fan, and C. Gmachl, IEEE Photon. J. **2**(3), 500–509 (2010).
[22]M. D. Escarra, A. J. Hoffman, K. J. Franz, S. S. Howard, R. Cendejas, X. Wang, J. Fan, and C. Gmachl, Appl. Phys. Lett. **94**, 251114 (2009).
[23]J. Faist, F. Capasso, C. Sirtori, D. L. Sivco, A. Y. Cho, L. Pfeiffer, and K. West, Solid-State Electron. **37**, 1273–1276 (1994).